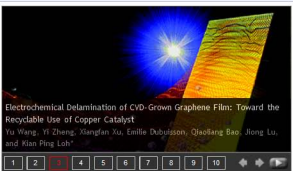




Search	Citation	DOI	Subject Search	Advanced Search
		Anywhere	Search	
<input checked="" type="radio"/> ACS Nano	<input type="radio"/> All Publications/Website			

Subscriber access provided by NATIONAL UNIV OF SINGAPORE

[Browse the Journal](#) • [Articles ASAP](#) • [Current Issue](#) • [Multimedia](#) • [Submission & Review](#) • [Subscriptions](#) • [About](#)
2010 Impact Factor **9.865**

Editor-in-Chief: Paul S. Weiss

- » Editors & EAB
- » About the Journal
- » Author Index
- » Recommend This Journal



Advertisements

Don't miss your chance to...

Info for Advertisers

## Browse By Issue

- Select Decade
- Select Volume
- Select Issue

List of Issues

GO

[Just Accepted](#) [Articles ASAP](#) [Current Issue](#)
[Most Read](#) [Most Cited](#)
[RSS feed](#)

## Most Read Articles

Now showing 1-5

[View All](#)

Most Read articles are updated on a monthly basis and available as 1 month and 12 month lists. Below is a Top 5 excerpt from the 1 month list.

 Select All For Selected Content: [View Abstracts](#) [Download Citations](#) [Hide All Thumbnails](#)

Au/Ag Bilayered Metal Mesh as a Si Etching Catalyst for Controlled Fabrication of Si Nanowires [Abstract](#) [Supporting Info](#)

Quantitative Biological Surface Science: Challenges and Recent Advances [Abstract](#)

Electrochemical Delamination of CVD-Grown Graphene Film: Toward the Recyclable Use of Copper Catalyst [Abstract](#) [Supporting Info](#)

Yu Wang, Yi Zheng, Xiangfan Xu, Emilie Dubuisson, Qiaoliang Bao, Jiang Lu, and Kian Ping Loh

2011, 5 (12), pp 9927-9933

Publication Date (Web): October 30, 2011 (Article)

DOI: 10.1021/nm203700w

Section: [Electrochemistry](#)

Fused Silver Nanowires with Metal Oxide Nanoparticles and Organic Polymers for Highly Transparent Conductors [Abstract](#) [Supporting Info](#)

Significant Efficiency Enhancement of Hybrid Solar Cells Using Core–Shell Nanowire Geometry for Energy Harvesting [Abstract](#) [Supporting Info](#)

Full Text HTML

[View all of the Most Read Articles](#)

## Materials SCENE

**materials SCENE**

A Flexible Power Source From Soot  
January 5, 2012

Polymerization Goes Tubular  
January 1, 2012

A Tunnel Into Cells  
January 1, 2012

[More SCENE Articles](#)

[C&EN Latest News](#)

## Connect with ACS Nano

» Twitter

## Audio/Podcast

Subscribe to the free ACS Nano monthly podcast.

» [Go to Audio/Podcast](#)

**ACS Nanotation**

Visit ACS Nanotation and see what experts in the field are saying about the latest research in nanoscience and nanotechnology!

Connect with ACS Nanotation:

Discover the Most Trusted Research Free!



Info for Advertisers

# Electrochemical Delamination of CVD-Grown Graphene Film: Toward the Recyclable Use of Copper Catalyst

Yu Wang,<sup>†</sup> Yi Zheng,<sup>†</sup> Xiangfan Xu,<sup>‡</sup> Emilie Dubuisson,<sup>†</sup> Qiaoliang Bao,<sup>†</sup> Jiong Lu,<sup>†</sup> and Kian Ping Loh<sup>†,\*</sup>

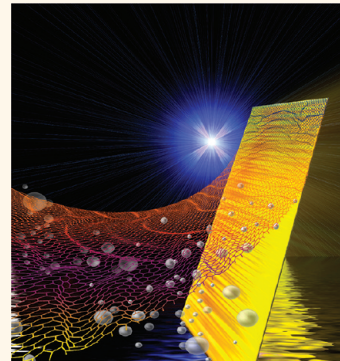
<sup>†</sup>Department of Chemistry, National University of Singapore, 3 Science Drive 3, 117543 Singapore and <sup>‡</sup>Department of Physics, National University of Singapore, 2 Science Drive 3, 117542 Singapore

**G**raphene, with its unique linear energy dispersion in which charge particles mimic massless Dirac fermions, exhibits extraordinary physical and electronic properties.<sup>1,2</sup> In particular, large-area, high-quality graphene film grown by chemical vapor deposition (CVD) method is promising for industrial applications because of its flexibility, high transparency, and electrical conductivity.<sup>3–5</sup> However, conventional methods of delaminating graphene from the metal substrates usually include a chemical etching step to remove the metal.<sup>6–8</sup> The etching step not only increases the production cost but also requires long treatment cycles of several hours. In principle, it should be possible to peel graphene from Cu foils by exerting external forces, similar to the mechanical exfoliation of graphene.<sup>2</sup> The interaction between graphene and Cu is relatively weak with a low binding energy of 33 meV per carbon atom,<sup>9,10</sup> comparable to the interplanar coupling strength of graphite (25 meV per carbon atom).<sup>11</sup> Here, we demonstrate a nondestructive route to delaminate graphene film from Cu foil by electrochemical means. The advantage of this technique is the industrial scalability of the process, as well as the reusability of the Cu foil in multiple growth and delamination cycles.

## RESULTS AND DISCUSSION

In a typical electrochemical delamination, a polymer (poly(methyl methacrylate) (PMMA)) layer was first spin-coated on graphene/Cu samples as a protection layer. During the electrochemical etching, direct current (dc) voltage is applied to the PMMA/graphene/Cu cathode and a glassy carbon anode in the electrolytic cell (Figure 1a). An aqueous solution of  $K_2S_2O_8$  (0.05 mM) was employed as electrolyte in the electrochemistry process. The graphene/Cu electrode was cathodically

**ABSTRACT** The separation of chemical vapor deposited (CVD) graphene from the metallic catalyst it is grown on, followed by a subsequent transfer to a dielectric substrate, is currently the adopted method for device fabrication. Most transfer techniques use a chemical etching method to dissolve the metal catalysts, thus imposing high material cost in large-scale fabrication. Here, we demonstrate a highly efficient, nondestructive electrochemical route for the delamination of CVD graphene film from metal surfaces. The electrochemically delaminated graphene films are continuous over 95% of the surface and exhibit increasingly better electronic quality after several growth cycles on the reused copper catalyst, due to the suppression of quasi-periodical nanoripples induced by copper step edges. The electrochemical delamination process affords the advantages of high efficiency, low-cost recyclability, and minimal use of etching chemicals.



**KEYWORDS:** graphene · electrochemical delamination · nondestruction · recyclability · nanoripple

polarized at  $-5\text{ V}$ , and hydrogen bubbles emerge at the graphene/Cu interfaces due to the reduction of water:  $2\text{H}_2\text{O(l)} + 2\text{e}^- \rightarrow \text{H}_2\text{(g)} + 2\text{OH}^-(\text{aq})$ . These  $\text{H}_2$  bubbles provide a gentle but persistent force to detach the graphene film from the Cu foil at its edges, and the process is aided by the permeation of the electrolyte solution into the interlayers as the edges delaminate (Figure 1b,c). Competing chemical etching and electrochemical deposition occurred on the electrode surface. In the presence of the etchant, a small degree of dissolution of the Cu foil occurs by this reaction:  $\text{Cu(s)} + \text{S}_2\text{O}_8^{2-}(\text{aq}) \rightarrow \text{Cu}^{2+} + 2\text{SO}_4^{2-}(\text{aq})$ . Simultaneously, local alkalization induced by hydroxyl ions produced from the dissociation of water precipitates  $\text{CuO}$  and  $\text{Cu}_2\text{O}$  on the copper foil by this reaction:  $3\text{Cu}^{2+}(\text{aq}) + 4\text{OH}^-(\text{aq}) + 2\text{e}^- \rightarrow \text{Cu}_2\text{O(s)} + \text{CuO(s)} + 2\text{H}_2\text{O(l)}$ .<sup>12,13</sup> The surface oxidation

\* Address correspondence to chmlohp@nus.edu.sg.

Received for review September 27, 2011 and accepted October 29, 2011.

Published online October 30, 2011  
10.1021/nn203700w

© 2011 American Chemical Society

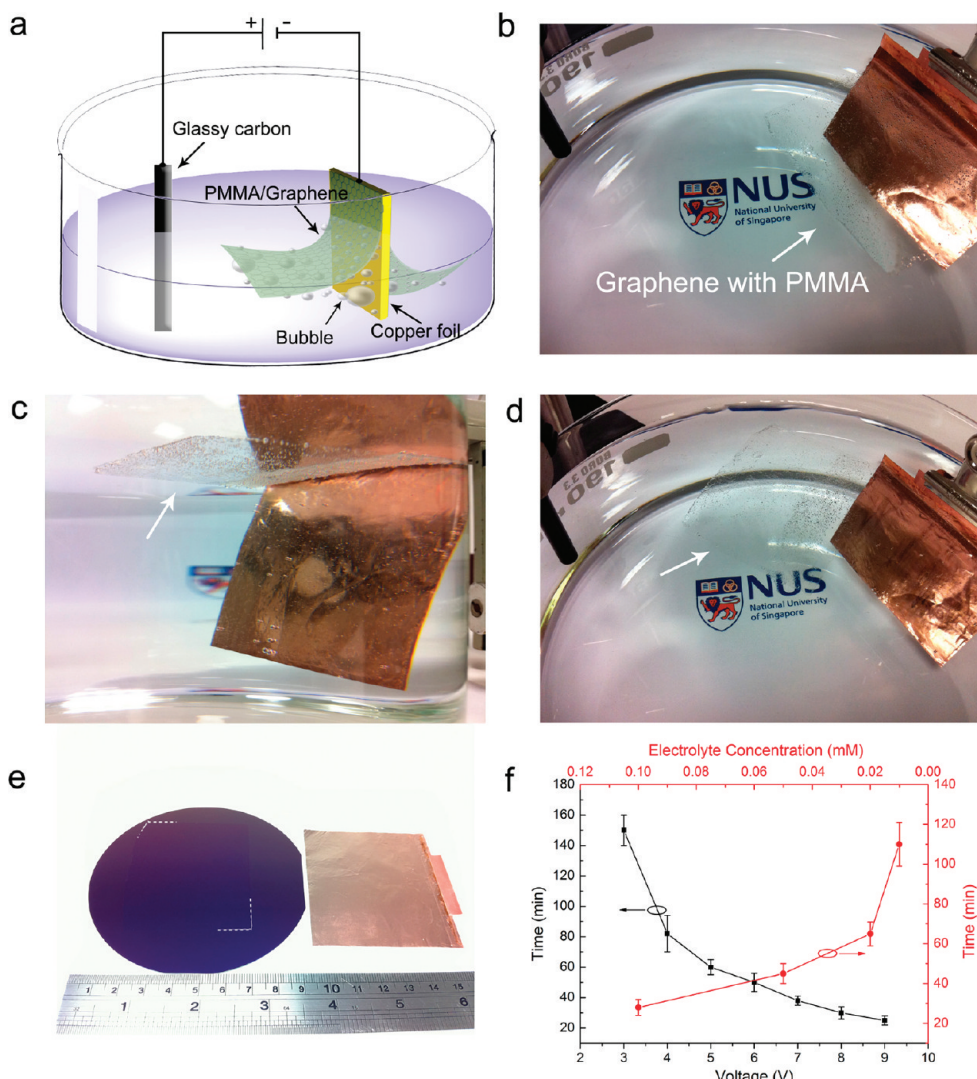


**Figure 1.** Electrochemical exfoliation of graphene from Cu foil. (a) Schematic diagram of electrochemical cell used for the electrochemical exfoliation. (b–d) Optical images showing the “whole film” peeling of PMMA-covered graphene from the copper foil. (e) Graphene film was transferred onto a 4 inch wafer by the wetting transfer process. (f) Curve showing time needed for complete film exfoliation of a 5 cm × 5 cm foil as a function of voltage (at 0.02 mM, black line) and electrolyte concentration (at 5 V, red line), respectively.

and electrodeposition of CuO and Cu<sub>2</sub>O passivate the Cu film from further chemical etching. XPS analysis shows that the Cu foil at the graphene–Cu interface after CVD growth is oxygen-free (XPS data, Figure S1 in the Supporting Information). Once the graphene film is delaminated, copper oxide appears on the surface. Using atomic force microscopy (AFM), we determine the thickness of the Cu film that is etched for each growth–delamination–transfer cycle to be less than 40 nm (Supporting Information). Taking the mass loss of Cu by evaporation (~30 nm/h at 1000 °C) during the CVD growth into account, this method will allow hundreds of cycles of repeated growth and delamination for a 25 μm thick Cu foil. In terms of efficiency, it is much higher than the standard etching–transferring techniques. The graphene/PMMA stack can be readily separated from Cu foil and transferred to the desired

substrate within 60 min (Figure 1d,e). In principle, the time of the electrochemical exfoliation can be controlled by the cathode voltage and the concentration of electrolyte (Figure 1f).

We found that the PMMA coating of the graphene is very important for a “clean” delamination of the graphene from the Cu foil. The PMMA layer acts as a supporting scaffold so that the graphene film will not roll or tear during the peeling process. In its absence, the peeled off graphene sheets are easily torn by shear force due to bubbling, and these fragmented sheets have a tendency to scroll up instantly once they are released, as shown in Figure 2a,b. In the presence of the PMMA protecting layer, the entire graphene/PMMA layer can be delaminated cleanly, as verified by AFM and SEM images of the Cu foil in Figure 2c,d, as well as Raman analysis of the Cu foil in Figure 2e. The efficiency

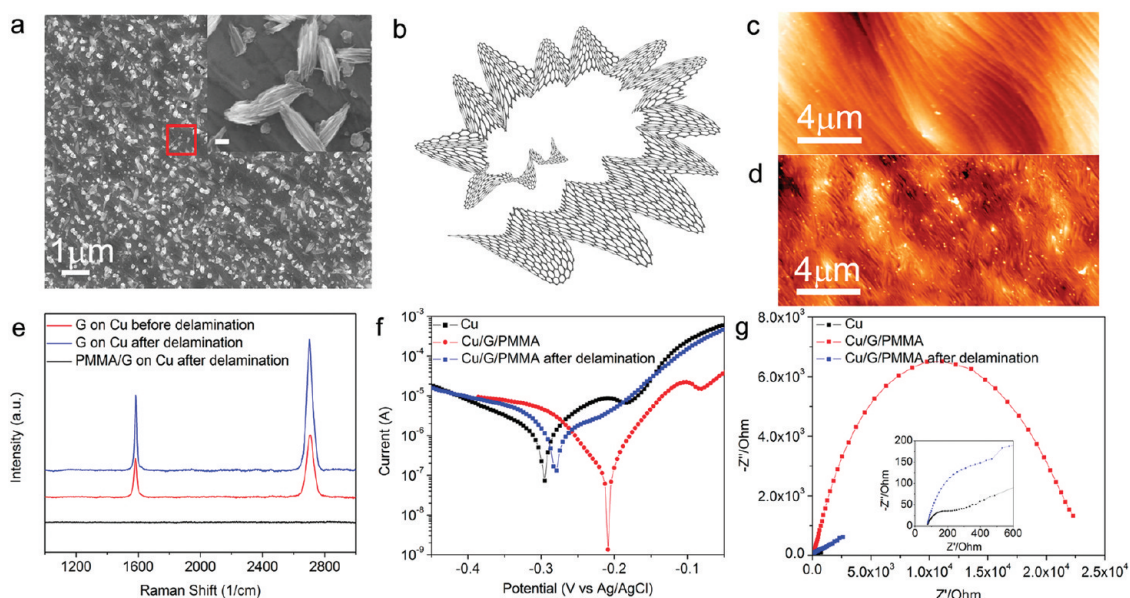


**Figure 2.** Role of PMMA layer. (a) SEM image of G on Cu foil without PMMA protection layer shows that the graphene film is broken up into scrolled sheets after electrochemical delamination. The inset is a magnified SEM image of the graphene scrolls. Scale bar is 100 nm. (b) Schematic drawing of graphene scroll corresponding to the inset of figure (a). (c) AFM image of Cu/G surface, showing a high density of single crystal terraces and step edges. (d) AFM image of Cu surface after one cycle of CVD growth and electrochemistry exfoliation. The surface becomes noticeably smoother due to etching and electrodeposition of Cu nanoparticles. Note that Cu nanoparticles may aggregate into big sizes of a few hundred nanometers, forming a random distribution on the Cu foil surface. No residual graphene patches are detected, which are typically a few micrometers in dimension. This indicates that graphene has been peeled off completely. (e) Raman comparison of Cu/G with and without PMMA samples before and after electrochemical delamination, respectively. (f,g) Tafel plot and impedimetric curves for G/Cu with and without PMMA protection layer, respectively.

of electrochemical exfoliation can be monitored by measuring the potentiostatic corrosion current in the form of Tafel plot, as shown in Figure 2f. When the Cu foil is protected by the graphene/PMMA stack, the corrosion is inhibited. Once the graphene/PMMA stack is peeled off, the corrosion current of the Cu foil increases sharply and the intersection point of the Tafel plot shifts from the corrosion potential of the graphene/PMMA-passivated Cu film (red line) to that of the bare Cu (black line). Electrochemical impedance analysis of the electrochemical charge transfer resistance, which can be judged from the diameter of the semiarc in the Nyquist plot, provides further evidence of the peeling process (Figure 2g). The intact PMMA/graphene/Cu stack has a large charge transfer resistance on account of the resistive protecting overlayer, whereas effective delamination of the PMMA/graphene/Cu stack produces a depressed loop in the Nyquist plot which is similar to the bare Cu foil (detailed electrochemical analysis is in Supporting Information Figures S2 and S3).

The physical morphology and electronic properties of CVD graphene film produced in three successive growth–delamination–transfer cycles were analyzed carefully to monitor the quality of the transferred film. In all three cycles, the CVD graphene film produced is highly continuous (>95%) as observed under the optical microscope (500 $\times$  magnification). AFM imaging of CVD graphene transferred onto SiO<sub>2</sub> for three successive cycles reveals distinct improvement in the surface

morphology. As shown in Figure 3a–c, CVD graphene produced in the first cycle (G1) is characterized by a high density of quasi-periodical nanoripples. In the second cycle (G2), the density of nanoripples in the CVD graphene film grown and delaminated from the same Cu foil is now much reduced, and the third cycle film (G3) shows an even greater reduction in the nanoripples' density. The reduction in the density of quasi-periodical nanoripple arrays from G1 to G3 leads to pronounced changes in the electronic properties of CVD graphene. The Raman spectra (532 nm excitation) in Figure 3d show that the quality of graphene film in each cycle improves, manifested by increasingly lower defect intensity, improved 2D-to-G ratio and narrowed full-width-at-half-maximum of the 2D peak.<sup>14,15</sup> The trend of reduced defect concentration as a function of growth cycles becomes more revealing when the D/G ratios are calculated by integrating the area of the D and G band for 400 spectra taken randomly. The D/G ratios of G1 and G2 have broader distribution, which are centered at  $\sim$ 0.18 and  $\sim$ 0.10, respectively, whereas G3 has a much narrower distribution of D/G ratio centered at  $\sim$ 0.082.

In line with the Raman measurements which show that the defect density decreases with each electrochemical delamination and transfer cycle, improvement in charge carrier mobility was observed with each cycle. As shown in Figure 3f, statistics tested on 15 samples for each delamination and transfer cycle

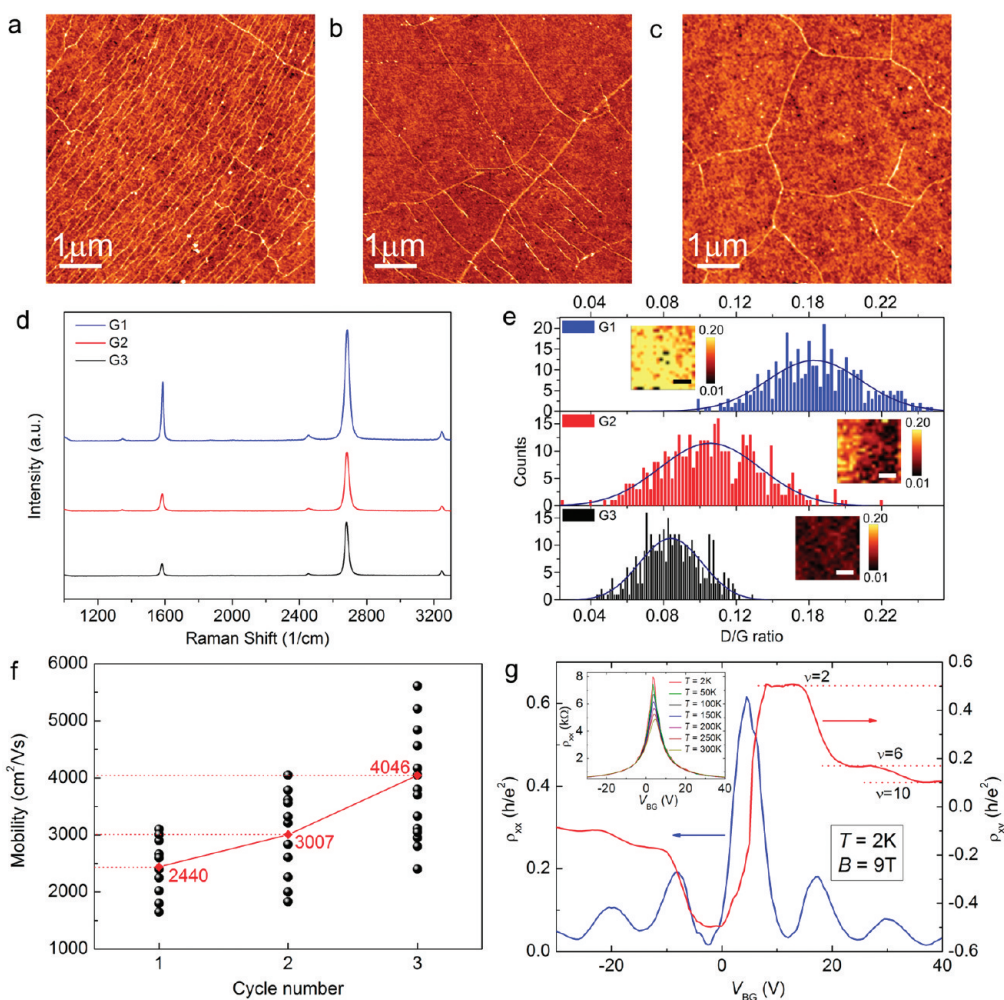


**Figure 3.** Morphology evolution of graphene films with three successive cycles of growth and electrochemical delamination and their electrical properties. (a–c) AFM images of graphene film delaminated by the electrochemistry process, showing the reduction of nanoripple density from G1 to G3 (G1, G2, and G3 refers to the first, second, and third cycles of electrochemical delamination). (d) Raman spectra of graphene film grown on the same copper foil catalyst for three circles. (e) Statistical histogram of the D/G ratio with Gaussian fits. It is derived from 400 Raman spectra which were point-by-point measured in the mapping area. The insets show Raman D/G maps with an area of  $10 \times 10 \mu\text{m}^2$ . Scale bar: 3  $\mu\text{m}$ . (f) Carrier mobility as a function of the cycle number of graphene growth. The red line is an average value of statistical mobility. (g) Quantum Hall effect at  $T = 2 \text{ K}$  and  $B = 9 \text{ T}$  for the G3 sample. The first three half-integer plateaus with  $\nu = 2, 6$ , and  $10$  are the fingerprint of single-layer graphene. The inset shows standard bipolar field effect and the increment of resistivity with temperature from 2 to 300 K, respectively.

clearly reveal a trend of enhancement in the field-effect mobility from  $2440 \text{ cm}^2 \text{ V}^{-1} \text{ s}^{-1}$  for G1,  $3007 \text{ cm}^2 \text{ V}^{-1} \text{ s}^{-1}$  for G2, to  $4046 \text{ cm}^2 \text{ V}^{-1} \text{ s}^{-1}$  for G3, as quasi-periodical nanorippling in CVD graphene is gradually suppressed. For a typical doping level of  $10^{12} \text{ cm}^{-2}$ , the mobility enhancement translates into an effective reduction in resistivity from  $2500 \Omega$  for G1 to  $1600 \Omega$  for G3. In general, the sheet resistance of graphene is determined by  $\rho = \rho_{\text{LRS}} + \rho_{\text{RS}} + \rho_{\text{LAPS}} + \rho_{\text{FPS}}$ , in which LRS, RS, LAPS, and FPS represent long-range Coulomb scattering,<sup>16</sup> resonant short-range scattering,<sup>17,18</sup> longitudinal acoustic phonon scattering,<sup>19</sup> and flexural phonon scattering induced by nanorippling and partial suspension,<sup>20,21</sup> respectively. At room temperature, LAPS is a constant and FPS sets an upper limit of  $\sim 10000 \text{ cm}^2 \text{ V}^{-1} \text{ s}^{-1}$  in mobility.<sup>21</sup> In theory, the resistivity

change by fully suppressing FPS can be empirically estimated as  $\Delta\rho_{\text{FPS}} = 1/ne\mu \sim 650 \Omega$ , which qualitatively agrees with the sheet resistance change of  $\sim 900 \Omega$  from G1 to G3. The noticeable difference between  $\Delta\rho_{\text{FPS}}$  and the experimental results indicates that, although the release of quasi-periodic nanoripples is the predominant origin for the mobility enhancement, nanorippling also contributes significantly to RS and LRS because local deformation can induce strain and modify the chemical reactivity, as supported by the Raman D band evolution in Figure 3d. The high quality of CVD graphene transferred is further verified by quantum Hall effect (QHE) measurements at 2 K and in 9 T magnetic fields. As shown in Figure 3g, the fingerprinting anomalous quantization sequences of  $\rho_{xy} = \pm(h/4e^2)/(n + 1/2) = h/ve^2$  for monolayer graphene are consistently observed for all

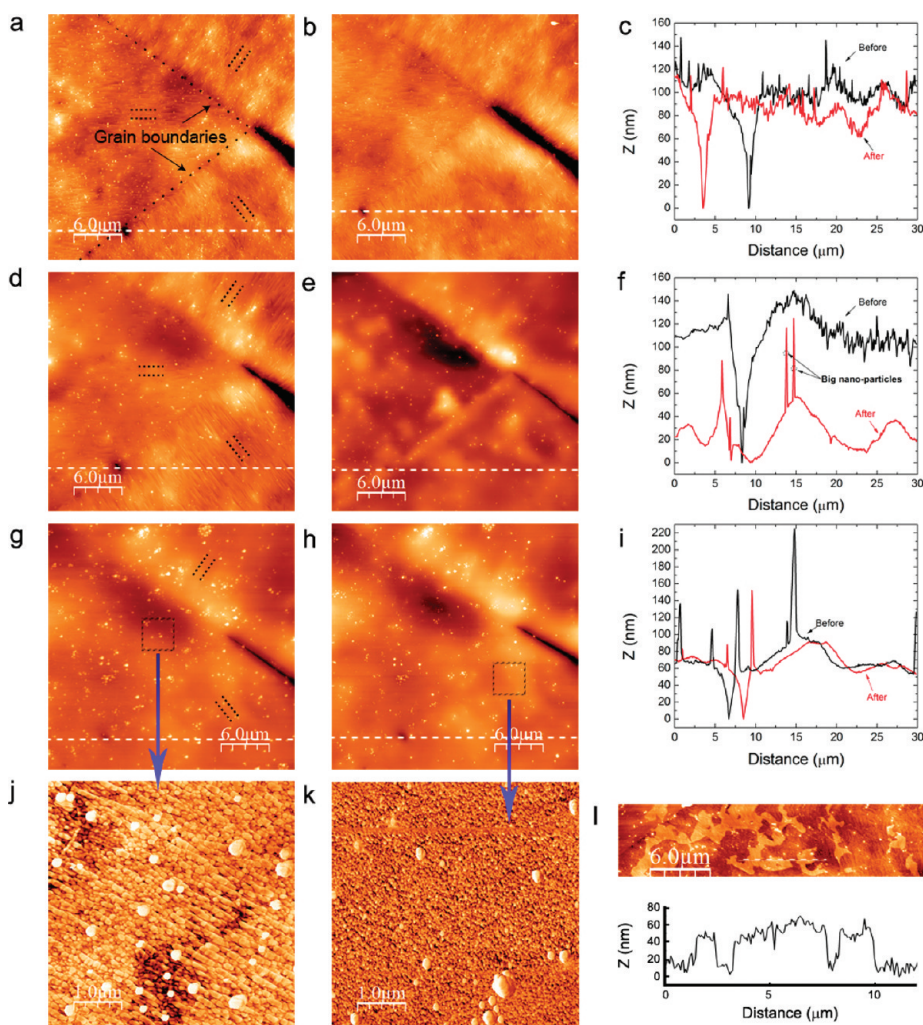


**Figure 4.** AFM measurements of the copper foil after three successive growth and electrochemical delamination cycles. (a–c) First growth–electrochemical delamination cycle. Cu foils show the characteristic grain boundary and step edge structures; spikes are due to copper nanoparticles; (d–f) second delamination cycle. The etching and restructuring gradually removes step edges and grain boundaries, followed by the electrodeposition of Cu nanoparticles which fill trenches and concavities. (g–i) Characteristic high-density terrace and step edge structures are not discernible anymore after three delamination cycles, and the Cu foil is covered uniformly by Cu nanoparticles. (j,k) AFM phase images of the regions in figure (g) and (h), respectively. (l) Thickness of the Cu foil has decreased by 40 nm after the electrochemical exfoliation, as judged from height differences between the bare (etched) region and a region that is passivated by graphene (using the conditions for partial etching).

three successive cycles. Thus, the transport measurements indicate that the topological symmetry of the graphene films grown in different cycles is not affected by the existence of nanoripples, while the electric properties can be improved by the release of the extrinsic ripples.

The observed evolution of the ripple release from G1 to G3 and the corresponding improvement in electronic properties have their origin in the step reconstruction of the Cu catalyst during multiple growth cycles, as revealed by the change in the surface topography of the Cu foil as a function of growth cycles (Figure 4). In the first circle, the surface of the Cu foil has a high density of terraces and step edges after CVD growth (Figure 4a–c), due to surface reconstruction and local melting at the CVD growth temperature of 1000 °C, which is close to the melting point of Cu.

These unique surface reconstructions of the Cu foil were imprinted onto graphene growing over it and preserved by the PMMA during the transfer process in a “microimprint” fashion onto the SiO<sub>2</sub> substrate. Therefore, the high density of quasi-periodical nano-ripple arrays on graphene originates from the local terraces and step edge structures on the Cu foil. During the multiple electrochemical etching and heating cycles, the Cu surface becomes increasingly smooth as step edges and grain boundaries are preferentially etched and the electrodeposition of Cu nanoparticles fills trenches and concavities (Figure 4g,h).

## CONCLUSION

From the viewpoint of Cu catalyst recycling, the electrochemical delamination method described here provides an economical and efficient way of preparing

high-quality CVD graphene for large-scale applications. The self-improvement inherent in the process arising from the electrochemical polishing and thermal restructuring of the copper foil is especially encouraging for the multiple reuse of the copper foil. In addition, this nondestructive method can be applied for the growth and transfer of graphene on polished single crystal without sacrificing the costly crystal, thus affording the possibility of producing high-quality graphene using a single-crystal substrate. We also discover that topographical features like ripples on the copper foil can be transferred to graphene, suggesting the possibilities to engineer 3-D strained structures by imprint lithography using

the topographical features created on the Cu substrate as the mold, followed by electrochemical peeling. The electrochemical delamination technique can be potentially integrated with polymer stamp-transfer imprint lithography. For example, a certain polymer can first be coated onto the graphene grown on copper, and this is followed by the electrochemical delamination of the copper foil; thereafter, the polymer-graphene stack can be stamp transferred onto any substrates. In conclusion, our work has explored the premise of electrochemical exfoliation as a viable and low-cost alternative to chemical etching of Cu and shows its promise for the transfer of high-quality monolayer graphene film.

## METHODS

**Chemical Vapor Deposition.** In a typical experiment, the CVD growth of graphene was carried out in a quartz tube at reduced pressure. Before the growth of graphene, the copper foil ( $25\text{ }\mu\text{m}$  thick, 99.999% purity) was preannealed at  $960\text{ }^\circ\text{C}$  for 8 h under a flow of  $\text{H}_2 = 50\text{ sccm}$  in order to prepare a high-density terrace structure on Cu. After that, the system was slowly cooled to room temperature ( $30\text{ }^\circ\text{C/h}$ ) under  $\text{H}_2$ . For CVD of graphene, the temperature was increased to  $1000\text{ }^\circ\text{C}$  under  $\text{H}_2$  (10 sccm). A gas mixture of  $\text{CH}_4$  (40 sccm) and  $\text{H}_2$  (10 sccm) was used for the growth of graphene at  $\sim 3.5$  Torr. After 25 min of growth, the system was cooled to room temperature under  $\text{H}_2$ .

**Characterization.** Surface morphology examination of graphene film and Cu foil was conducted by tapping-mode AFM using an XE-100 system from Park Systems. STM measurements with a SPECS Aarhus 150 system were performed in an ultrahigh-vacuum (UHV) chamber at a base pressure of  $2 \times 10^{-10}$  mbar. The Raman spectroscopy was carried out on a WITec alpha300 S confocal Raman system with laser source of 532 nm. The laser power is controlled below 2 mW to avoid heating damage to graphene samples. For the Raman mapping, the scanning area is  $10 \times 10\text{ }\mu\text{m}^2$  with a lateral resolution of 500 nm ( $20 \times 20$  pixels).

For the resistance measurement, a small ac current (10 nA) was applied through the samples and the longitudinal and transverse voltage was measured using a Stanford 830 lock-in amplifier. The samples were made into Hall bar geometry by standard e-beam lithography technique with the length of  $3.5\text{ }\mu\text{m}$  between source and drain. The highly doped silicon wafer is served as the gate electrode with a 300 nm silicon oxide as the dielectric layer. The charge density in graphene is induced by applying a gate voltage through a Keithley 6430 source meter. The room temperature resistance is measured in probe station (Alessi REL-4800) in four-contact configurations. Low-temperature magnetoresistance is measured in Cryogenic 9T variable temperature system from 2 to 300 K.

The electrochemical corrosion study was carried out in a polytetrafluoroethylene (PTFE) cell (volume is around 5 mL). The exposed surface area is a circle (diameter = 4 mm). The working electrode (the copper sample) was clamped tightly at the base of the PTFE housing. A Ag/AgCl (in saturated KCl) electrode and a Pt wire were used as the reference and auxiliary electrodes, respectively. The electrochemical measurements were carried out using an Autolab PGSTAT30 digital potentiostat/galvanostat with FRA2 module.

**Acknowledgment.** We thank the financial support of the NRF-CRP award "Graphene and Related Materials and Devices" (R-143-000-360-281). We thank Prof. Barbaros Ozyilmaz for use of electrical measurement facilities.

**Supporting Information Available:** Supplementary methods and figures. This material is available free of charge via the Internet at <http://pubs.acs.org>.

## REFERENCES AND NOTES

- Neto, A. H. C.; Guinea, F.; Peres, N. M. R.; Novoselov, K. S.; Geim, A. K. The Electronic Properties of Graphene. *Rev. Mod. Phys.* **2009**, *81*, 109–162.
- Geim, A. K.; Novoselov, K. S. The Rise of Graphene. *Nat. Mater.* **2007**, *6*, 183–191.
- Li, X.; Cai, W.; An, J.; Kim, S.; Nah, J.; Yang, D.; Piner, R.; Velamakanni, A.; Jung, I.; Tutuc, E.; et al. Large-Area Synthesis of High-Quality and Uniform Graphene Films on Copper Foils. *Science* **2009**, *324*, 1312–1314.
- Kim, K.; Zhao, Y.; Jang, H.; Lee, S.; Kim, J. M.; Kim, K. S.; Ahn, J.-H.; Kim, P.; Choi, J.-Y.; Hong, B. H. Large-Scale Pattern Growth of Graphene Films for Stretchable Transparent Electrodes. *Nature* **2009**, *457*, 706–710.
- Reina, A.; Jia, X.; Ho, J.; Nezich, D.; Son, H.; Bulovic, V.; Dresselhaus, M. S.; Kong, J. Large Area, Few-Layer Graphene Films on Arbitrary Substrates by Chemical Vapor Deposition. *Nano Lett.* **2009**, *9*, 3087–3087.
- Bae, S.; Kim, H.; Lee, Y.; Xu, X.; Park, J.; Zheng, Y.; Balakrishnan, J.; Lei, T.; Kim, H. R.; Song, Y.; et al. Roll-to-Roll Production of 30-Inch Graphene Films for Transparent Electrodes. *Nat. Nanotechnol.* **2010**, *5*, 574–578.
- Li, X. S.; Zhu, Y. W.; Cai, W. W.; Borysiak, M.; Han, B.; Chen, D.; Piner, R. D.; Colombo, L.; Ruoff, R. S. Transfer of Large-Area Graphene Films for High-Performance Transparent Conductive Electrodes. *Nano Lett.* **2009**, *9*, 4359–4363.
- Lee, Y.; Bae, S.; Jang, H.; Jang, S.; Zhu, S.; Sim, S. H.; Song, Y.; Hong, B. H.; Ahn, J. Wafer-Scale Synthesis and Transfer of Graphene Films. *Nano Lett.* **2010**, *10*, 490–493.
- Giovannetti, G.; Khomyakov, P. A.; Brocks, G.; Karpan, V. M.; Brink, J.; Kelly, P. J. Doping Graphene with Metal Contacts. *Phys. Rev. Lett.* **2008**, *101*, 026803.
- Gao, L.; Guest, J. R.; Guisinger, N. P. Epitaxial Graphene on Cu(111). *Nano Lett.* **2010**, *10*, 3512–3516.
- Schabel, M. C.; Martins, J. L. Energetics of Interplanar Binding in Graphite. *Phys. Rev. B* **1992**, *46*, 7185–7188.
- de Jongh, P. E.; Vanmaekelbergh, D.; Kelly, J. J. Cu<sub>2</sub>O: Electrodeposition and Characterization. *Chem. Mater.* **1999**, *11*, 3512–3517.
- Thimsen, E.; Paracchino, A.; Laporte, V.; Sivula, K.; Gratzel, M. Highly Active Oxide Photocathode for Photoelectrochemical Water Reduction. *Nat. Mater.* **2011**, *10*, 456–461.
- Saito, R.; Jorio, A.; Souza Filho, A. G.; Dresselhaus, G.; Dresselhaus, M. S.; Pimenta, M. A. Probing Phonon Dispersion Relations of Graphite by Double Resonance Raman Scattering. *Phys. Rev. Lett.* **2002**, *88*, 027401.
- Casiraghi, C.; Pisana, S.; Novoselov, K. S.; Geim, A. K.; Ferrari, A. C. Raman Fingerprint of Charged Impurities in Graphene. *Appl. Phys. Lett.* **2007**, *91*, 233108.
- Ando, T. Screening Effect and Impurity Scattering in Monolayer Graphene. *J. Phys. Soc. Jpn.* **2006**, *75*, 074716.

17. Ni, Z. H.; Ponomarenko, L. A.; Nair, R. R.; Yang, R.; Anissimova, S.; Grigorieva, I. V.; Schedin, F.; Blake, P.; Shen, Z. X.; Hill, E. H.; *et al.* On Resonant Scatterers as a Factor Limiting Carrier Mobility in Graphene. *Nano Lett.* **2010**, *10*, 3868–3872.
18. Wehling, T. O.; Yuan, S.; Lichtenstein, A. I.; Geim, A. K.; Katsnelson, M. I. Resonant Scattering by Realistic Impurities in Graphene. *Phys. Rev. Lett.* **2010**, *105*, 056802.
19. Efetov, D. K.; Kim, P. Controlling Electron-Phonon Interactions in Graphene at Ultrahigh Carrier Densities. *Phys. Rev. Lett.* **2010**, *105*, 256805.
20. Katsnelson, M. I.; Geim, A. K. Electron Scattering on Microscopic Corrugations in Graphene. *Philos. Trans. R. Soc., A* **2008**, *366*, 195–204.
21. Castro, E. V.; Ochoa, H.; Katsnelson, M. I.; Gorbachev, R. V.; Elias, D. C.; Novoselov, K. S.; Geim, A. K.; Guinea, F. Limits on Charge Carrier Mobility in Suspended Graphene Due to Flexural Phonons. *Phys. Rev. Lett.* **2010**, *105*, 266601.

## SUPPLEMENTARY INFORMATION

# Electrochemical Delamination of CVD Grown Graphene Film: Toward the Recyclable Use of Copper Catalyst

Yu Wang,<sup>†</sup> Yi Zheng,<sup>†</sup> Xiangfan Xu,<sup>‡</sup> Emilie Dubuisson,<sup>†</sup> Qiaoliang Bao,<sup>†</sup> Jiong Lu,<sup>†</sup> and Kian Ping

Loh<sup>†,\*</sup>

<sup>†</sup> *Department of Chemistry, National University of Singapore, 3 Science Drive 3, 117543, Singapore*

<sup>‡</sup> *Department of Physics, National University of Singapore, 2 Science Drive 3, 117542, Singapore*

\*E-mail: chmlohkp@nus.edu.sg

**Voltammetric experiments.** The relationship between current density and potential of anodic and cathodic electrode reactions under kinetics controlled by the charge transfer is given by the Butler-Volmer equation [1,2]:

$$I = i_0 \cdot \left\{ \exp \left[ \frac{(1-\alpha)nF}{RT} (E - E_{corr}) \right] - \exp \left[ -\frac{\alpha nF}{RT} (E - E_{corr}) \right] \right\}$$

where the over potential,  $\eta = E - E_{corr}$

$I$ : electrode current, A;

$i_0$ : exchange current density, A/m<sup>2</sup>;

$E$ : electrode potential, V;

$E_{corr}$ : corrosion potential, V;

$A$ : electrode active surface area, m<sup>2</sup>;

$T$ : the absolute temperature, K;

$n$ : number of electrons involved in the electrode reaction;

$F$ : Faraday constant;

$R$ : universal gas constant;

$\alpha$ : the symmetry factor or charge transfer coefficient, dimensionless;

The corrosion current and potential can be determined from the Tafel Slope Analysis. The electrochemical exfoliation efficiency has been followed by two different electrochemical studies: linear sweep voltammetry (LSV) and electrochemical impedance spectroscopy (EIS).

## Figures

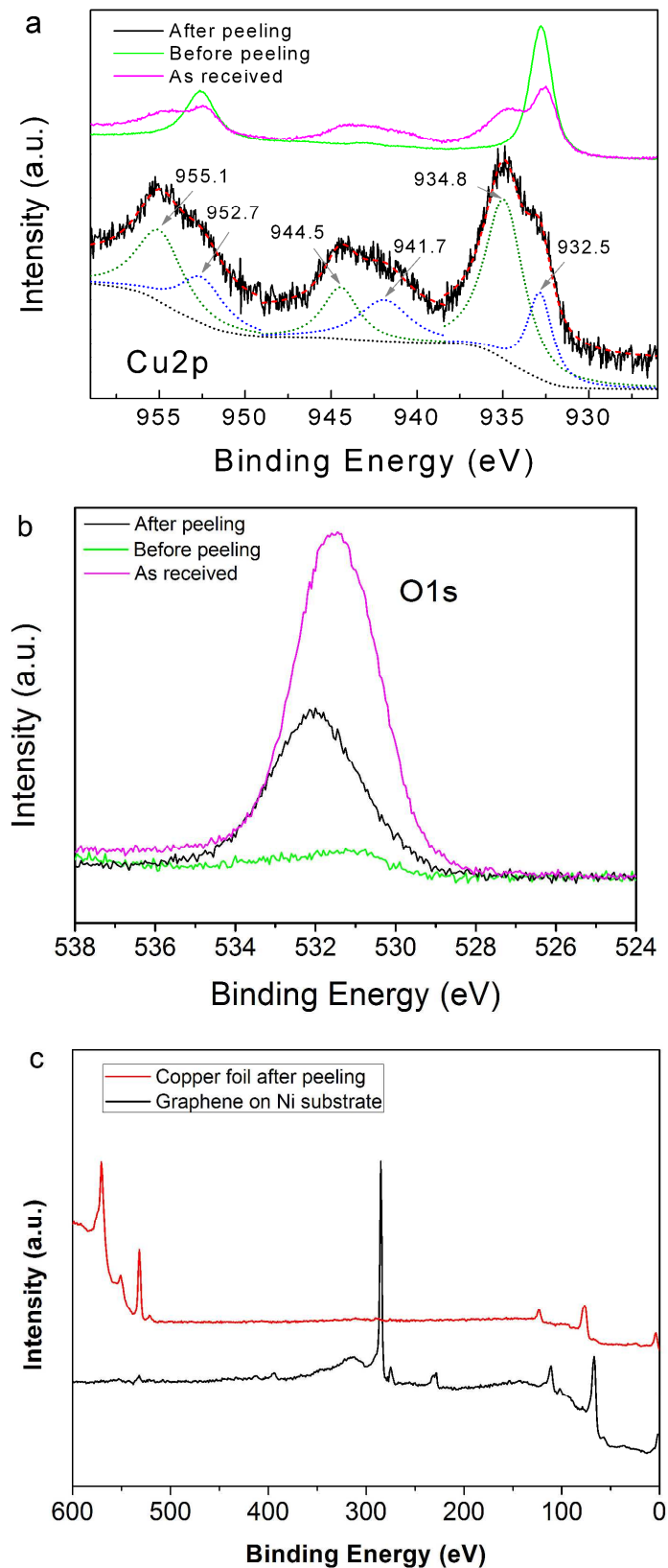


**Figure S1.** XPS measurements of the surface of copper foil. (a) Cu 2p XPS spectra measured on the Cu foil before (solid green line) and after the electrochemical exfoliation (solid black line). The sample As received is shown as a pink line. (b) O 1s XPS spectra measured on the Cu foil before (solid green line) and after the electrochemical exfoliation (solid black line). The sample As received is shown as a pink line. (c) Full XPS spectrum showing Intensity (a.u.) vs Binding Energy (eV) from 600 to 0 eV. It compares Copper foil after peeling (red line) and Graphene on Ni substrate (black line).

after electrochemical exfoliation was blown dry by  $N_2$  gas and immediately loaded into XPS chamber. CuO is characterized by two peaks (941.7 and 944.5 eV) between the bulk Cu  $2p_{3/2}$  (932.5 eV) and Cu  $2p_{1/2}$  (952.7 eV) peaks, respectively. After the separation of graphene from the Cu foil *via* the electrochemistry process, chemically shifted peaks appear on the higher energy side (934.8 and 955.1 eV) of the main bulk Cu  $2p_{3/2}$  and Cu  $2p_{1/2}$ , indicating CuO formation. Simultaneously, CuO satellite peaks appear around 944.5. This confirms the existence of a CuO layer on the Cu foil after the electrochemical exfoliation process. (b) Oxygen  $2p$  XPS spectra measured on the Cu foil before (solid green line) and after the electrochemical exfoliation (solid black line). The appearance of oxygen state with  $E_b(O1s) = 531.9$  eV in the spectra also demonstrates the formation of CuO on the copper foil, agreeing with the analysis of Cu $2p$  spectra. Cu and oxygen  $2p$  XPS spectra of as-received Cu foil is also shown (solid magenta line) for comparison. Note that electrochemically etched Cu and air-oxidized Cu show distinct core level shifts and intensities. The amount of electrochemically deposited copper oxide, as judged from the chemically shifted Cu peak as well as O $1s$  peak intensity, is about 20% of the oxide thickness on air-exposed Cu foil. (c) XPS survey scan of copper substrate and graphene film transferred onto Ni substrate. The result shows no residual copper on the graphene film. The small oxygen signal on nickel is due to nickel oxide.

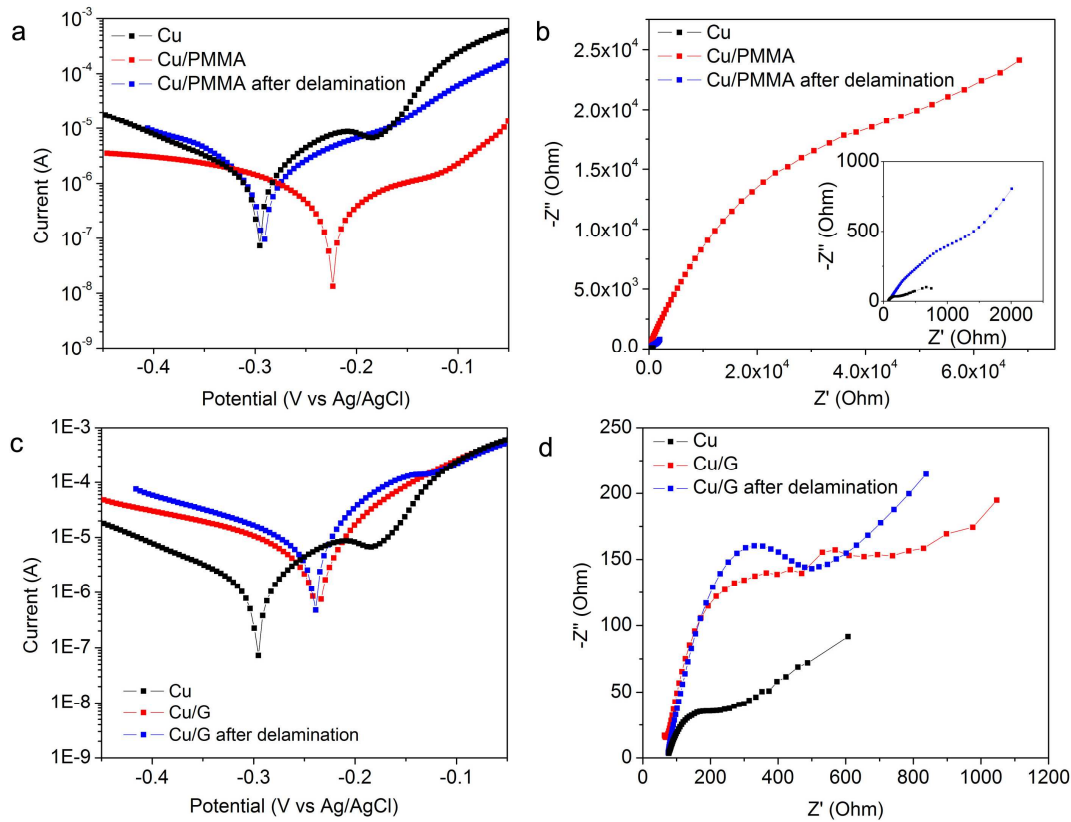


**Figure S2.** The role of PMMA from the control experiments. (a) and (b) Polarization and impedimetric curves of Cu and Cu/PMMA before and after the electrochemical delamination, showing the PMMA layer acts as a corrosion inhibitor. (c) and (d) Polarization and impedimetric curves of Cu and Cu/G, showing no significant change for the Cu/G sample before and after the electrochemical delamination, indicating that the Cu foil is still coated largely by G.

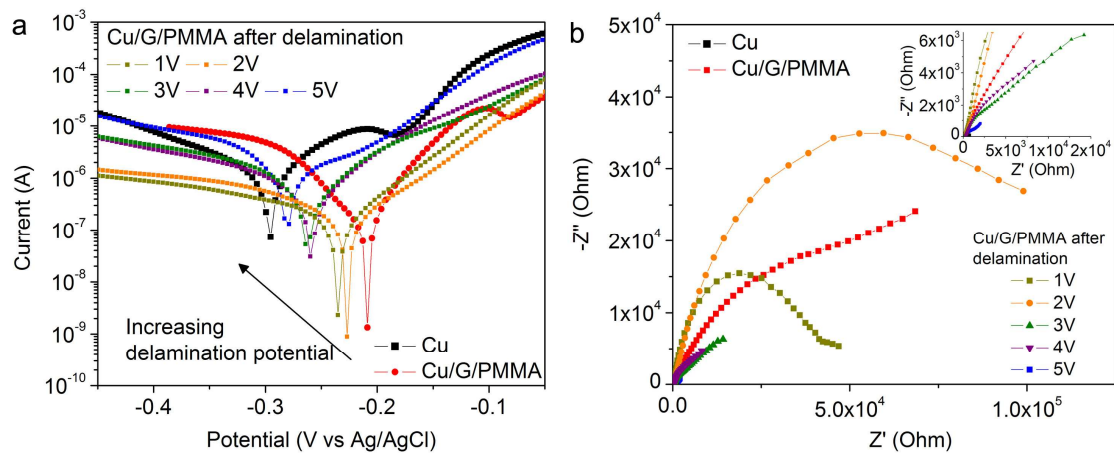


**Figure S3.** Effect of potential on the electrochemistry delamination. (a) Linear sweep voltammetry curves show that the higher the electrode voltage is, the more  $E_{corr}$  moves towards more negative potential. The corrosion current increases above 3V. (b) For 1V and 2V etching, the charge transfer resistance  $R_{ct}$  increases, whereas for 3, 4 and 5V,  $R_{ct}$  decreases. For electrode potentials  $< 3$  V, the bubbling is not strong enough to remove the PMMA/G films. Above 3V, the film is removed and the  $R_{ct}$  decreases.

**Table 1.** By extrapolating the Tafel anodic and cathodic linear parts until they intersect as straight lines, the corrosion current ( $I_{\text{corr}}$ ), corrosion potential ( $E_{\text{corr}}$ ), polarization resistance ( $R_p$ ), the anodic and cathodic Tafel slopes,  $\beta_a$  and  $\beta_c$ , can be deduced, respectively.

	$I_{\text{corr}}$ (A/cm <sup>2</sup> )	$\beta_c$ (V/dec)	$\beta_a$ (V/dec)	$R_p$ ( $\Omega$ )	$E_{\text{corr}}$ (V)
Cu	6.14E-04	0.129	0.081	3.79E+03	-0.296
Cu/G/PMMA	4.41E-05	0.027	0.043	5.76E+03	-0.208
Cu/G/PMMA after delamination	4.61E-04	0.115	0.069	3.81E+03	-0.281
Cu/PMMA	8.38E-05	0.066	0.066	1.14E+04	-0.224
Cu/PMMA after delamination	3.49E-04	0.069	0.073	3.20E+03	-0.292
Cu/G	7.49E-04	0.059	0.034	5.96E+02	-0.237
Cu/G after delamination	1.96E-03	0.092	0.038	3.96E+02	-0.240

The Nyquist plot exhibits a charge transfer loop, the charge transfer resistance can be judged from the diameter of the loop. At high frequency, the curves were fitted using an equivalent circuit modeling:  $R_s - R_{\text{ct}}/\text{CPE}$ . The parameters are listed in Table 2.  $R_s$  is the solution resistance.  $R_{\text{ct}}$  represents the charge-transfer resistance and is inversely proportional to corrosion rate.  $R_{\text{ct}}$  is in parallel with the constant phase element, CPE.

**Table 2.**

	$R_s$ ( $\Omega$ )	$R_{\text{ct}}$ ( $\Omega$ )	CPE (F)	$n$
Cu	7.30E+01	1.69E+02	7.96E-04	0.47
Cu/G/PMMA	1.97E+02	2.06E+04	5.30E-06	0.72
Cu/G/PMMA after delamination	7.35E+01	4.55E+02	8.04E-05	0.65
Cu/PMMA	5.00E+01	5.63E+04	4.70E-06	0.52
Cu/PMMA after delamination	8.59E+01	2.06E+03	1.85E-04	0.43
Cu/G	6.64E+01	4.15E+02	8.48E-05	0.71
Cu/G after delamination	7.30E+01	5.56E+02	1.59E-04	0.65

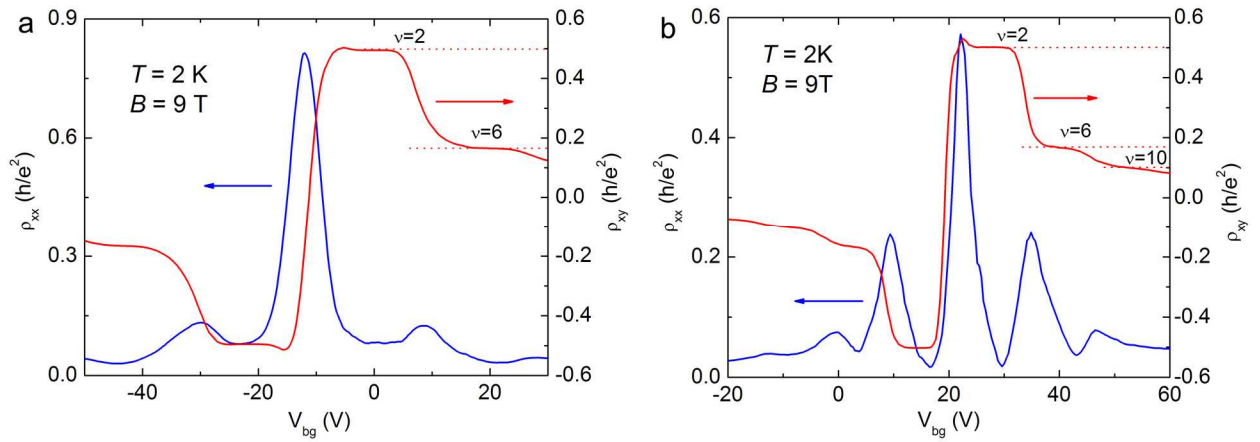


**Figure S4.** Quantum Hall effect for G1 and G2 samples at  $T = 2\text{ K}$  and  $B = 9\text{ T}$ . Graphene samples prepared by three successive electrochemical delamination all shows the fingerprinting quantization sequences of  $\pm(h/4e^2)/(n+1/2)$  for monolayer graphene.

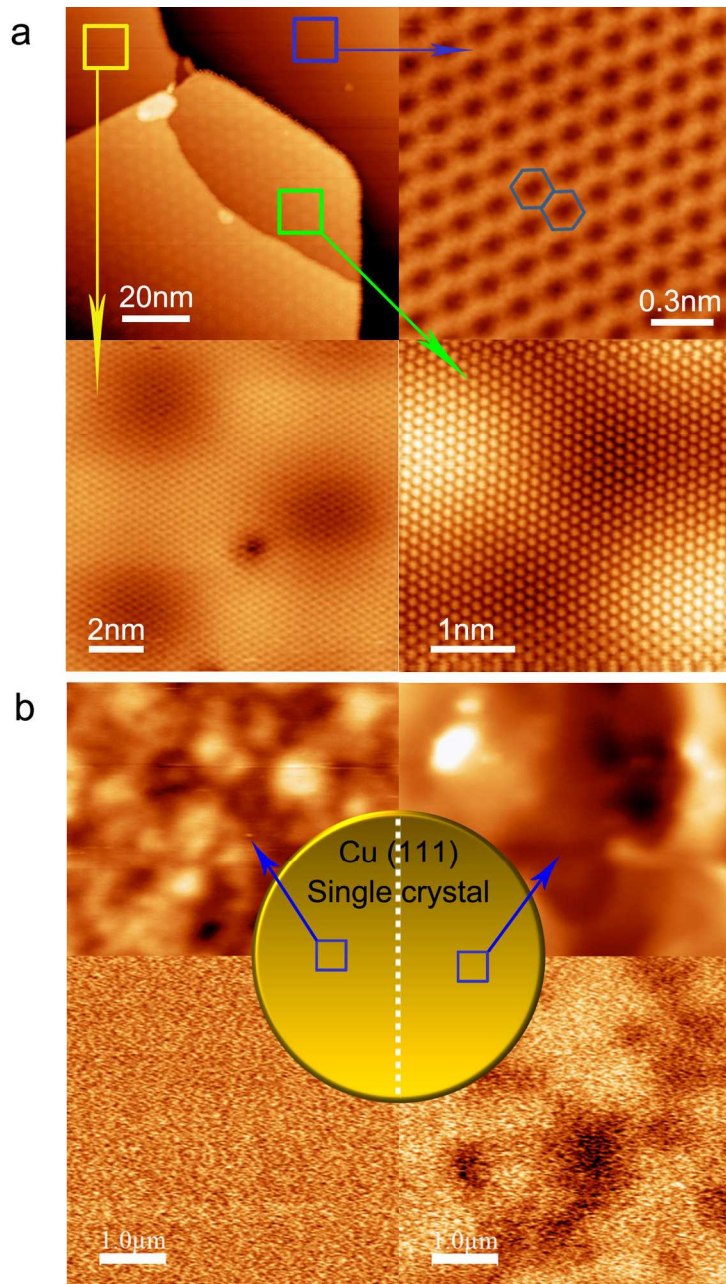


**Figure S5.** Surface of the Cu (111) single crystal before and after electrochemistry delamination. (a) Before the electrochemical delamination, STM analysis shows that the Cu (111) single crystal was covered by high quality graphene monolayer exhibiting honeycomb lattice (blue square region), as well as bilayer with Moiré pattern (yellow square region) and intermediate structure with triangular-lattice (green square region) graphene film. (b) For comparison, the graphene film at the left half of single crystal was peeled off, while the right portion still has graphene on the surface of Cu (111). From AFM

phase images, the graphene film can be completely exfoliated by the electrochemical process.

## References

1. Bockris, J. O'M.; Reddy, A. K. N.; Gamboa-Aldeco, M. *Modern Electrochemistry 2A. Fundamentals of Electrodics* 2nd Edn (Kluwer Academic/Plenum Publishers, **2000**)
2. Bard, A.; Faulkner, L. *Electrochemical Methods. Fundamentals and Applications* 2<sup>nd</sup> Edn (John Wiley and Sons, Inc., **2001**)

# Electrochemical Delamination of CVD Grown Graphene Film: Toward the Recyclable Use of Copper Catalyst

Yu Wang,<sup>†</sup> Yi Zheng,<sup>†</sup> Xiangfan Xu,<sup>‡</sup> Emilie Dubuisson,<sup>†</sup> Qiaoliang Bao,<sup>†</sup> Jiong Lu,<sup>†</sup> and Kian Ping Loh<sup>†,\*</sup>

<sup>†</sup> Department of Chemistry, National University of Singapore, 3 Science Drive 3, 117543, Singapore

<sup>‡</sup> Department of Physics, National University of Singapore, 2 Science Drive 3, 117542, Singapore

\*E-mail: chmlohp@nus.edu.sg

